Ottolenghi, M. (1980) *Adv. Photochem. 12*, 97-200.
Ovchinnikov, Y. A., Abdulaev, A. S., Zolotarev, A. S., Artamonov, I. D., Bespalov, I. A., Dergachev, A. E., & Tsuda, M. (1988) *FEBS Lett. 232*, 69-72.
Palings, I., Pardoen, J., van den Berg, E., Winkel, C., Lugtenburg, J., & Mathies, R. (1987) *Biochemistry 26*, 2544-2556.
Pande, C., Pande, A., Yue, K. T., Callender, R. H., Ebrey, T. G., & Tsuda, M. (1987) *Biochemistry 26*, 4941-4947.
Rimai, L., Heyde, M. E., & Gill, D. (1973) *J. Am. Chem. Soc. 95*, 4493-4501.
Rothschild, K., Cantore, W., & Marrero, H. (1983) *Science 219*, 1333-1335.
Rothschild, K. J., Roepe, P., Ahl, P. L., Earnest, T. N., Bogolmoni, R. A., Das Gupta, S. K., Mulliken, C. M., & Herzfeld, J. (1986) *Proc. Natl. Acad. Sci. U.S.A. 83*, 347-351.
Schick, G. A., Cooper, T. M., Holloway, R. A., Murray, L. P., & Birge, R. R. (1987) *Biochemistry 26*, 2556-2562.
Siebert, F., Maentele, W., & Gerwert, K. (1983) *Eur. J. Biochem. 136*, 119-127.
Smith, S. O., Myers, A. B., Mathies, R. A., Pardoen, J. A., Winkel, C., van den Berg, E. M. M., & Lugtenburg, J. (1985) *Biophys. J. 47*, 653-664.
Stryer, L. (1986) *Annu. Rev. Neurocsi, 9*, 87-119.
Suzuki, T., Uji, K., & Kito, Y. (1976) *Biochim. Biophys. Acta 428*, 321-338.
Tsuda, M. (1979) *Biochim. Biophys. Acta 545* 537-546.
Tsuda, M. (1982a) *Methods Enzymol. 81*, 392-399.
Tsuda, M. (1982b) *Methods Enzymol. 88*, 552-561.
Tsuda, M. (1987) *Photochem. Photobiol. 45*, 915-931.
Tsuda, M., Tokunaga, F., Ebrey, T., Yue, K. T., Marque, J., & Eisenstein, L. (1980) *Nature (London) 287*, 461-462.
Yoshizawa, T. (1972) in *Handbook of Sensory Physiology—Photochemistry of Vision* (Dartnell, H. J. A., Ed.) Springer-Verlag, New York.
Yoshizawa, T., & Wald, G. (1964) *Nature (London) 221*, 340-345.

NMR Studies of Abasic Sites in DNA Duplexes: Deoxyadenosine Stacks into the Helix Opposite Acyclic Lesions†

Matthew W. Kalnik,‡ Chien-Neng Chang,§ Francis Johnson,§ Arthur P. Grollman,*,§ and Dinshaw J. Patel*,‡

Department of Biochemistry and Molecular Biophysics, College of Physicians and Surgeons, Columbia University, New York, New York 10032, and Department of Pharmacological Sciences, State University of New York at Stony Brook, Stony Brook, New York 11794-8651

Received September 16, 1988; Revised Manuscript Received December 1, 1988

ABSTRACT: Proton and phosphorus NMR studies are reported for two complementary nonanucleotide duplexes containing acyclic abasic sites. The first duplex, d(C-A-T-G-A-G-T-A-C)·d(G-T-A-C-*P*-C-A-T-G), contains an acyclic propanyl moiety, P, located opposite a deoxyadenosine at the center of the helix (designated AP_P 9-mer duplex). The second duplex, d(C-A-T-G-A-G-T-A-C)·d(G-T-A-C-*E*-C-A-T-G), contains a similarly located acyclic ethanyl moiety, E (designated AP_E 9-mer duplex). The ethanyl moiety is one carbon shorter than the natural carbon–phosphodiester backbone of a single nucleotide unit of DNA. The majority of the exchangeable and nonexchangeable base and sugar protons in both the AP_P 9-mer and AP_E 9-mer duplexes, including those at the abasic site, have been assigned by recording and analyzing two-dimensional phase-sensitive NOESY data sets in H_2O and D_2O solution between −5 and 5 °C. These spectroscopic observations establish that A5 inserts into the helix opposite the abasic site (P14 and E14) and stacks between the flanking G4·C15 and G6·C13 Watson–Crick base pairs in both the AP_P 9-mer and AP_E 9-mer duplexes. The helix is right-handed at and adjacent to the abasic site, and all glycosidic torsion angles are anti in both 9-mer duplexes. Proton NMR parameters for the AP_P 9-mer and AP_E 9-mer duplexes are similar to those reported previously for the AP_F 9-mer duplex (F = furan) in which a cyclic analogue of deoxyribose was embedded in an otherwise identical DNA sequence [Kalnik, M. W., Chang, C. N., Grollman, A. P., & Patel, D. J. (1988) *Biochemistry 27*, 924-931]. These proton NMR experiments demonstrate that the structures at abasic sites are very similar whether the five-membered ring is open or closed or whether the phosphodiester backbone is shortened by one carbon atom. Phosphorus spectra of the AP_P 9-mer and AP_E 9-mer duplexes (5 °C) indicate that the backbone conformation is similarly perturbed at three phosphodiester backbone torsion angles. These same torsion angles are also distorted in the AP_F 9-mer but assume a different conformation than those in the AP_P 9-mer and AP_E 9-mer duplexes.

Abasic sites in DNA are created by the loss of a purine or pyrimidine residue (Lindahl, 1982; Loeb & Preston, 1987; Weiss & Grossman, 1987). Such lesions, which arise spontaneously or through the action of *N*-glycosylases, lack primary coding information. Unless repaired prior to DNA replication, apurinic/apyrimidinic (AP) sites promote misincorporation of nucleotides and mutagenesis (Loeb & Kunkel, 1982; Loeb, 1985). The presence of AP sites in DNA also leads to strand scission via β-elimination (Weiss & Grossman, 1987).

In naturally occurring AP sites, a dynamic equilibrium exists between the cyclic hemiacetal (structure 1) and open-chain aldehyde (structure 2) forms of the 2-deoxyribose residue.

†This research was supported by NIH Grants CA-46533 to D.J.P. and CA-17395 and ES-04068 to A.P.G. NMR studies were conducted on instrumentation purchased with funds provided by Robert Woods Johnson Jr. Charitable Trust and the Matheson Foundation.
‡Columbia University.
§State University of New York at Stony Brook.

0006-2960/89/0428-3373$01.50/0

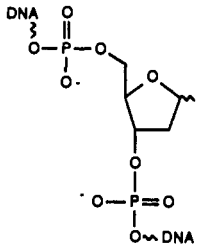

Structure 1

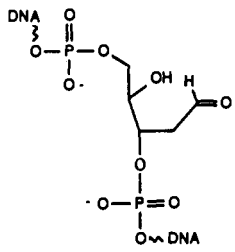

Structure 2

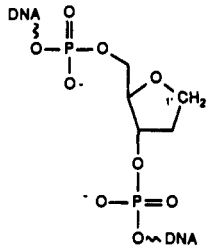

Structure 3

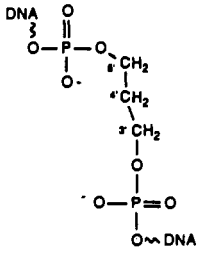

Structure 4

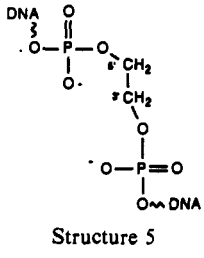

Structure 5

Cyclic (structure 3) and acyclic (structure 4) forms, representing chemically stable analogues of the hemiacetal and aldehyde forms, respectively, have been incorporated into oligodeoxynucleotides and shown to serve as substrates for several AP endonucleases and DNA polymerases (Takeshita et al., 1987). In the present study, a disubstituted propane analogue, P (structure 4), was introduced into the phosphodiester backbone at the center of a complementary oligodeoxynucleotide duplex, d(C-A-T-G-*A*-G-T-A-C)·d(G-T-A-C-*P*-C-A-T-G) (structure 6, designated AP_P 9-mer duplex), in which deoxyadenosine is located opposite the acyclic abasic site. The carbon atoms of the propane moiety (P) correspond

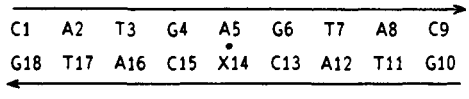

A5·F14	Structure 6
A5·P14	Structure 7
A5·E14	Structure 8
A5·T14	Structure 9

to the 3-, 4-, and 5-carbons of the 2-deoxyribose of the natural abasic site. A disubstituted ethane analogue, E (structure 5), in which the carbon–phosphodiester backbone is shortened by one carbon atom, has also been inserted at the same position of an otherwise identical nonamer duplex (structure 7, designated AP_E 9-mer duplex). In vitro studies demonstrate that DNA polymerase is blocked at the ethanyl and propanyl sites.

The structures of the AP_P 9-mer and AP_E 9-mer duplexes in solution have been probed by two-dimensional NMR experiments. These NMR results are compared with analogous studies of the parent A·T 9-mer duplex (structure 8) and the tetrahydrofuran (F, structure 3) analogue containing duplex (structure 9, designated AP_F 9-mer duplex), an analogue of the cyclic form of the natural (structure 1) abasic site (Kalnik et al., 1988).

Experimental Procedures

Oligonucleotide Synthesis. The preparation of the modified oligodeoxyribonucleotides containing synthetic abasic sites has been described elsewhere (Takeshita et al., 1987). Each nonanucleotide was assembled on a 5-μmol resin column with a Vega (Du Pont) Coder 300 automated DNA synthesizer. A protected dihydroxypropane or dihydroxyethane moiety (Takeshita et al., 1987) was incorporated at the appropriate position, forming the abasic site; the remaining protected nucleotides were then added. Coupling yields for each addition reaction were 98%.

Sample Preparations. A 1:1 stoichiometry of the complementary strands in the AP_P 9-mer duplex was achieved by monitoring the cytidine H6 proton resonances during the gradual addition of the d(C-A-T-G-*A*-G-T-A-C) strand to the d(G-T-A-C-*P*-C-A-T-G) strand at 45 °C. At this temperature the duplex is melted into single unstacked strands, and the narrow resonances can be used to generate 1:1 stoichiometry of the two strands. The duplex is annealed by lowering the temperature. NMR spectra of the AP_P 9-mer duplex were recorded on ~270 A_{260} units in 0.40 mL of 0.1 M NaCl–10 mM phosphate–1 mM EDTA solution with either 100% D_2O at pH 6.7 or 90% H_2O/10% D_2O (v/v) at pH 6.5. A 1:1 stoichiometry of the AP_E 9-mer duplex was obtained in a similar fashion. NMR spectra of the AP_E 9-mer duplex were recorded on ~220 A_{260} units in 0.40 mL of 0.2 M NaCl–20 mM phosphate–2 mM EDTA solution of 90% H_2O/10% D_2O (v/v) at pH 6.15 or in 0.40 mL of 0.1 M NaCl–10 mM phosphate–1 mM EDTA solution of 100% D_2O at pH 6.3. The pH values in D_2O are uncorrected pH readings.

NMR Experiments. One- and two-dimensional proton data sets were collected on a Bruker AM 500 spectrometer using quadrature detection. Proton chemical shifts are referenced to external TSP. One- and two-dimensional 121.5-MHz proton Waltz-decoupled (Shaka et al., 1982) phosphorus spectra were collected on a Bruker AM 300 spectrometer using quadrature detection. Phosphorus chemical shifts are referenced relative to external trimethyl phosphate (TMP). The two-dimensional data sets were collected as pure absorption phase spectra (States et al., 1982).

Phase-sensitive two-dimensional NOESY spectra of the AP_P 9-mer duplex in H_2O buffer were collected with a 120-ms mixing time and a 1.0-s repetition delay. A jump–return ($90y$, t_w, $90 - y$) solvent suppression pulse (Plateau & Gueron, 1982) was used for the preparation, acquisition, and detection pulses. The carrier frequency was centered on the H_2O signal, and the waiting time, t_w, was optimized for even exicitation of the imino and aromatic protons (65 μs). Each t_1 increment consists of 1024 complex data points collected with 256 scans and a sweep width of 10000 Hz in the t_2 dimension. The free induction decays were apodized with a 90°-shifted sine bell function zeroed at the 1024th point in the t_2 dimension and to the 256th point in the t_1 dimension and 3-Hz broadening in both dimensions. Each dimension was base-line corrected with a fifth-order polynomial base-line fitting routine supplied by Dr. Arthur Pardi (unpublished results) after Fourier transformation. The phase-sensitive two-dimensional NOESY spectrum of the AP_E 9-mer duplex was collected at a later date with an improved pulse scheme. The jump–return solvent suppression pulse was still used for detection, while the preparation and mixing pulses were replaced by ~70° hard pulses (~6.0 μs). The reduction from a 90° pulse allowed the receiver gain to be increased by at least a factor of 2,

significantly increasing the sensitivity (unpublished results). The acquisition and processing parameters for the AP_E 9-mer duplex are otherwise identical with those for the AP_P 9-mer duplex.

Magnitude two-dimensional correlated (COSY) experiments on the AP_P 9-mer and AP_E 9-mer duplexes in D_2O solution were collected with 512 t_1 increments and a sweep width of 5000 Hz from 1024 complex data points in the t_2 dimension. The magnitude COSY data were collected with 48 scans per t_1 increment and a repetition delay of 1.5 s. The data sets were apodized with an unshifted sine bell function zeroed at the 512th point and Fourier transformed in both dimensions.

Phase-sensitive two-dimensional nuclear Overhauser effect (NOESY) spectra were collected on the AP_P 9-mer and AP_E 9-mer duplexes in D_2O solution with a mixing time of 250 ms and similar parameters as given for the COSY experiments. The NOESY data were apodized with a 90°-shifted sine bell function zeroed at the 1024th point in the t_2 dimension and to the 256th point in the t_1 dimension.

Phase-sensitive two-dimensional ^1H–^{31}P heteronuclear correlation experiments conducted upon the AP_P 9-mer duplexes utilize an MLEV-17 composite pulse scheme which achieves a net exchange of magnetization between coupled protons via a homonuclear Hartmann–Hahn (HOHAHA) type cross-polarization (Bax & Davis, 1985). This net magnetization transfer is then relayed to the ^{31}P atoms via an INEPT sequence (Zagorski & Norman, 1989). The carrier frequency was placed in the center of the 121.5-MHz phosphorus spectrum. The time domain data sets were accumulated over a sweep width of 300 Hz from 256 complex data points in the t_2 dimension. A sweep width of 2800 Hz was used in the t_1 dimension. A total of 77 t_1 increments were collected for the AP_P 9-mer duplex, and 116 t_1 increments were collected for the AP_E 9-mer. Each t_1 increment was collected with a 1.0-s repetition delay and 1024 scans per increment. Both dimensions were zero filled to 1024 complex data points prior to Fourier transformation. The t_2 dimension was apodized with a Gaussian multiplication of −1.0 Hz and 0.04-Hz broadening, and the t_1 dimension was apodized with 3-Hz line broadening.

Data Processing. The first t_1 increment of each NOESY spectrum was multiplied by 0.5 prior to Fourier transformation of the second dimension to suppress t_1 ridges (Otting et al., 1986). The average of the first 100 rows was subtracted from the entire COSY spectrum to reduce t_1 noise (Klevitt, 1985). One- and two-dimensional data sets were processed with FTNMR software (D. Hare, unpublished results) on a Vax 11-780 and a micro Vax II.

Results

AP_P 9-mer Duplex

Exchangeable Protons. The proton NMR spectrum of the AP_P 9-mer duplex in H_2O solution exhibits eight partially resolved imino resonances between 12.0 and 14.0 ppm at 0 °C. Four thymidine imino proton resonances are detected between 13.5 and 13.7 ppm, and four guanosine imino proton resonances are detected between 12.3 and 12.9 ppm. The exchangeable imino proton spectrum of the acyclic abasic analogue (structure 4) containing AP_P 9-mer duplex is nearly identical with the exchangeable imino proton spectrum of the acyclic abasic analogue (structure 3) containing AP_F 9-mer duplex (Kalnik et al., 1988). The imino protons of the AP_P 9-mer duplex broaden as the temperature is raised to 20 °C, reflecting the onset of the melting transition.

An analysis of the phase-sensitive NOESY spectrum (mixing time 120 ms) of the AP_P 9-mer duplex in H_2O solution

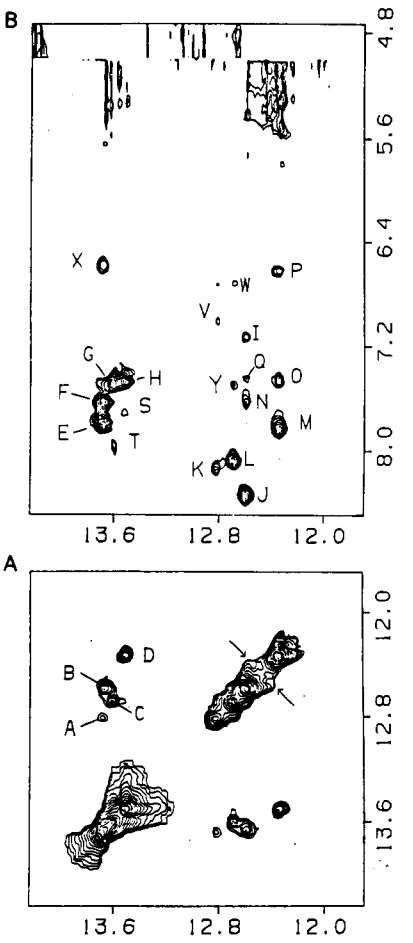

FIGURE 1: Expanded phase-sensitive NOESY (120-ms mixing time) contour plots of the AP_P 9-mer duplex in 0.1 M NaCl, 10 mM phosphate, and H_2O, pH 6.5, at 0 °C. (A) Crosspeaks establishing connectivities between imino protons in the symmetrical 12.0–14.0-ppm spectral range. (B) Crosspeaks establishing connectivities between the imino protons (12.0–14.0 ppm) and the base and amino protons (4.8–8.5 ppm). The crosspeaks A–X are assigned as follows: The 13.68-ppm imino proton of T17 exhibits NOE crosspeaks to the imino proton of G18 (peak A) and to the H2 proton (peak E) and exposed amino proton of A2 (peak X). The 13.66-ppm imino proton of T3 exhibits NOE crosspeaks to the imino proton of G4 (peak B) and to the H2 proton (peak F) and exposed amino proton of A16 (peak X). The NOE crosspeaks involving the thymidine imino proton and the adenosine hydrogen-bonded amino proton within the A2·T17 and T3·A16 base pairs resonate at the same positions as the NOE crosspeaks between the thymidine imino protons and the adenosine H2 protons within the same two base pairs (peaks E and F, respectively). The 13.60-ppm imino proton of T11 exhibits NOE crosspeaks to the imino proton of G10 (peak C) and to the hydrogen-bonded amino proton (peak T) and H2 proton of A8 (peak G). The 13.50-ppm imino proton of T7 exhibits NOE crosspeaks to the imino proton of G6 (peak D) and the hydrogen-bonded amino proton (peak S) and H2 proton (peak H) of A12. The 12.81-ppm imino proton of G18 exhibits NOE crosspeaks to the hydrogen-bonded (peak K) and exposed (peak V) amino protons of C1. The 12.69-ppm imino proton of G10 exhibits NOE crosspeaks to the hydrogen-bonded (peak L) and exposed (peak W) amino protons of C9 and to the H2 proton of A8 (peak Y). The 12.59-ppm imino proton of G4 exhibits NOE crosspeaks to the hydrogen-bonded (peak J) and exposed (peak I) amino protons of C15 and to the H2 protons of A16 (peak N) and A5 (peak Q). The 12.34-ppm imino proton of G6 exhibits NOE crosspeaks to the hydrogen-bonded (peak M) and exposed (peak P) amino protons of C13 and to the H2 protons of A5 (peak O) and A12 (peak O).

at 0 °C has yielded imino, cytidine amino, and adenosine amino proton assignments. The two regions of interest are expanded in Figure 1A, where crosspeaks represent distance connectivities between imino protons on adjacent base pairs (12.0–14.5 ppm), and in Figure 1B, where crosspeaks represent distance connectivities between imino protons and either cy-

Table I: Proton Chemical Shifts in the AP_P 9-mer Duplex

base pair	chemical shifts (ppm)[a] T-H3	G-H1	C-H4b	C-H4e	A-H2
C1·G18		12.82	8.14	7.03	
A2·T17	13.68				7.80
T3·A16	13.66				7.64
G4·C15		12.59	8.34	7.12	
A5·P14					7.44
G6·C13		12.34	7.84	6.63	
T7·A12	13.50				7.47
A8·T11	13.60				7.49
C9·G10		12.69	8.08	6.72	

base	chemical shifts (ppm)[b] H8	H2	H6	H5/CH_3	H1′	H2′	H2″	H3′	H4′
C1			7.67	5.89	5.65	2.0	2.41	4.69	4.03
A2	8.42	7.80			6.26	2.73	2.90	5.00	4.38
T3			7.14	1.45	5.60	1.88	2.21	4.78	4.09
G4	7.69				5.43	2.39	2.44	4.89	4.23
A5	7.94	7.44			5.38	2.41	2.50	4.84	4.25
G6	7.86				5.83	2.62	2.72	4.76	
T7			7.19	1.41	5.61	2.04	2.39	4.81	4.15
A8	8.22	7.52			6.23	2.63	2.84	4.98	4.40
C9			7.23	5.09	5.96	2.08	2.08	4.42	3.95
G10	7.85				5.88	2.60	2.72	4.77	4.18
T11			7.38	1.30	5.78	2.16	2.49	4.88	4.21
A12	8.27	7.49			6.19	2.65	2.85	5.01	4.39
C13			7.39	5.31	6.02	2.15	2.20	4.81	4.21
C15			7.75	6.02	5.76	2.12	2.49	4.86	4.26
A16	8.41	7.65			6.19	2.71	2.89	5.00	4.38
T17			7.12	1.48	5.72	1.82	2.25	4.78	4.08
G18	7.84				6.08	2.30	2.56	4.63	4.14

[a] 0.1 M NaCl, 10 mM phosphate, H_2O, pH 6.5, 0 °C; exchangeable protons. [b] 0.1 M NaCl, 10 mM phosphate, D_2O, pH 6.7, 5 °C; nonexchangeable protons.

tidine amino protons or adenosine H2 protons (7.2–8.5 ppm). The thymidine imino protons are assigned on the basis of their intra base pair NOEs to the H2 protons of adenosine which are selectively observed in an inversion–recovery experiment on the AP_P 9-mer duplex in D_2O solution. The H2 protons of adenosine are assigned on the basis of their distance connectivities with nearby assigned sugar H1′ protons (see next section). The four crosspeaks between the thymidine imino and adenosine H2 protons reflect Watson–Crick pairing in A2·T17, T3·A16, A8·T11, and T7·A12 base pairs (crosspeaks E–H, respectively, Figure 1B). The guanosine imino protons are then assigned by monitoring imino to imino NOE connectivities observed between adjacent base pairs (Figure 1A). Thus, crosspeaks A–D in Figure 1A are NOE connectivities between the imino protons of adjacent residues T17 and G18, T3 and G4, T11 and G10, and T7 and G6, respectively. The guanosine imino protons also display characteristic NOEs to the cytidine amino protons in Watson–Crick base pairs, allowing their assignment. Hence, crosspeaks J–M in Figure 1B represent intra base pair NOEs between the guanosine imino and hydrogen-bonded cytidine amino protons of the G4·C15, G18·C1, G10·C9, and G6·C13 base pairs, respectively. The exchangeable proton and adenosine H2 proton chemical shift assignments for the AP_P 9-mer in H_2O solution at 0 °C are listed in Table I.

Several other NOE connectivities are identified between the guanosine imino protons and the adenosine H2 protons on adjacent base pairs. The G4 imino proton displays NOEs to both flanking adenosine H2 protons of residues A16 and A5 (crosspeaks N and Q, respectively, Figure 1B). The G6 imino proton exhibits overlapping NOE crosspeaks to the flanking H2 protons of residues A12 and A5 (crosspeak O, Figure 1B). The imino proton of G10 displays a NOE to the adjacent H2 proton of residue A8 (crosspeak R, Figure 1B). The remaining crosspeaks S and T (Figure 1B) represent NOEs between thymidine imino protons and adenosine amino protons.

One-dimensional NOE difference spectra were recorded on the AP_P 9-mer duplex in H_2O solution at 0 °C following saturation of the G4 and G6 imino protons flanking the abasic site. These experiments confirm the observation that the H2 proton of the A5 residue opposite the acyclic propane abasic site develops NOEs to the G4 and G10 imino protons of the flanking G·C base pairs in the AP_P 9-mer duplex.

Nonexchangeable Protons. The nonexchangeable base and sugar protons in the AP_P 9-mer duplex have been assigned by analyzing the through-space connectivities obtained in a two-dimensional NOESY experiment and the through-bond connectivities obtained in a two-dimensional COSY experiment in D_2O solution at 5 °C according to established experimental procedures (Hare et al., 1983; Scheek et al., 1984; Weiss et al., 1984). An expanded region of the AP_P 9-mer duplex NOESY spectrum (mixing time 250 ms) outlining the distance connectivities between the base protons (7.0–8.5 ppm) and the sugar H1′ (5.2–6.4 ppm) and H3′ (4.4–5.1 ppm) protons is plotted in Figure 2A for the unmodified strand and in Figure 2B for the modified strand. The crosspeaks marked by an asterisk in Figure 2 are the fixed-distance NOE crosspeaks between the H5 and H6 protons of the four cytidine residues, two in each strand. Each purine H8 and pyrimidine H6 proton in regular right-handed DNA displays NOE crosspeaks to its own and 5′-neighboring sugar H1′, H2′, H2″, and H3′ protons. This directionality is used to identify adjacent base protons by stepping through their intervening sugar protons along each strand in the duplex. The unmodified strand can be traced from the C1 5′-terminus to the C9 3′-terminus without interruption at the G4-A5-G6 segment opposite the abasic site (Figure 2A). The tracing from the G10 5′-terminus to the G18 3′-terminus on the modified strand has an interruption at residue P14, the acyclic abasic site analogue, since none of the protons of residue P14 resonate between 4.4 and 8.5 ppm

Table II: Proton Chemical Shifts in the AP_E 9-mer Duplex

base pair	chemical shifts (ppm)[a] T-H3	G-H1	C-H4b	C-H4e	A-H2
C1·G18		12.75	8.14	6.92	
A2·T17	13.67				7.74
T3·A16	13.66				7.61
G4·C15		12.62	8.27	7.07	
A5·E14					7.46
G6·C13		12.30	7.79	6.59	
T7·A12	13.51				7.46
A8·T11	13.55				7.46
C9·G10		12.61	8.05	6.62	

base	chemical shifts (ppm)[b] H8	H2	H6	H5/CH_3	H1′	H2′	H2″	H3′	H4′
C1			7.70	5.94	5.63	2.03	2.43	4.71	4.05
A2	8.41	7.46			6.28	2.75	2.93	5.02	4.41
T3			7.17	1.48	5.63	1.91	2.23	4.81	4.11
G4	7.73				5.45	2.40	2.47	4.89	4.26
A5	7.99	7.46			5.41	2.45	2.52	4.87	4.26
G6	7.88				5.87	2.68	2.73	4.85	
T7			7.23	1.44	5.66	2.07	2.42	4.83	4.16
A8	8.26	7.35			6.26	2.66	2.86	5.01	4.41
C9			7.29	5.20	6.01	2.10	2.10	4.45	3.99
G10	7.90				5.93	2.65	2.75	4.78	4.20
T11			7.42	1.33	5.79	2.18	2.52	4.90	4.23
A12	8.28	7.32			6.21	2.67	2.86	5.03	4.40
C13			7.40	5.32	6.02	2.18	2.18	4.85	4.23
C15			7.76	6.05	5.76	2.10	2.48	4.87	4.27
A16	8.43	7.46			6.21	2.73	2.91	5.02	4.40
T17			7.14	1.51	5.74	1.84	2.28	4.80	4.08
G18	7.86				6.11	2.32	2.58	4.65	4.15

[a] 0.2 M NaCl, 20 mM phosphate, H_2O, pH 6.15, 0 °C; exchangeable protons. [b] 0.1 M NaCl, 10 mM phosphate, D_2O, pH 6.3, 5 °C; nonexchangeable protons.

(Figure 2B). The same directionality is observed for the NOEs between the purine H8/pyrimidine H6 protons and the sugar H3′ protons (4.4–5.1 ppm) on the same and 5′-flanking residues in the AP_P 9-mer duplex.

Other NOE crosspeaks are helpful in establishing assignments when two or more protons have identical chemical shifts. In right-handed DNA, NOE crosspeaks between purine H8 and pyrimidine H5/CH_3 protons on adjacent bases evolve at purine(3′–5′)pyrimidine steps. These base to base NOEs are exclusively observed for the A2-T3, G6-T7, A8-C9 (crosspeak A, Figure 2A), G10-T11, A12-C13 (crosspeak B, Figure 2B), and A16-T17 purine(3′–5′)pyrimidine steps in the AP_P 9-mer duplex. Adenosine H2 protons display directional NOEs to their own, 3′-linked and cross-strand sugar H1′ protons in right-handed duplex DNA. NOEs between adenosine H2 protons and their own sugar H1′ protons are observed for residues A5, A8, and A12 (crosspeaks J, F, and G, Figure 2A). The H2 proton of adenosine displays NOEs to the 3′-linked sugar H1′ proton in the A2-T3, A16-T17, A8-C9, and A12-C13 steps (crosspeaks C, D, E, and H, Figure 2A) and cross-strand NOEs between the H2 of residue A2 and the H1′ of residue T17 and between the H2 proton of residue A5 and the H1′ proton of residue C15 (crosspeaks J and K, respectively, Figure 2A).

The distance connectivities between base and sugar H1′, H2′, H2″, and H3′ protons provide a self-consistent check for assignment of the protons in the AP_P 9-mer duplex. Further confirmation of the assignments made above and throughout the NOESY spectrum is obtained by analyzing the sugar H1′, H2′, H2″, and H3′ coupling connectivities observed in the COSY spectrum. The nonexchangeable proton assignments for the AP_P 9-mer duplex in D_2O solution at 5 °C are tabulated in Table I.

The proton resonances of the abasic site propanyl moiety are numbered as they would be in an intact 2′-deoxyribose sugar as the H3′,3″, H4′,4″, and H5′,5″ protons (structure 4). The H3′,3″ and H5′,5″ protons of residue P14 are predicted to resonate between 3.5 and 5.0 ppm, analogous to the H5′,5″ protons of a normal 2′-deoxyribose embedded in a right-handed DNA duplex. The H4′,4″ protons are expected to resonate between 1.5 and 2.0 ppm typical of a methylene group bonded to two other carbons. An analysis of the expanded region involving these protons (3.5–5.0 ppm and 1.5–5.0 ppm) in the COSY and NOESY spectra indicates that the H4′,4″ protons are superimposed and resonate at 1.90 ppm, while the four H3′,3″ and H5′,5″ protons which are partially resolved resonate at 3.94 and 3.89 ppm (Table III). The H3′,3″ and H5′,5″ protons can be distinguished on the basis of heteronuclear correlations to the ^{31}P atoms in the phosphodiester backbone. These results are presented in the next section and demonstrate that the P14 H3′,3″ protons resonate at 3.89 ppm and the P14 H5′,5″ protons resonate at 3.94 ppm.

Table III: ^{31}P–^1H Heteronuclear Correlations and ^{31}P Chemical Shifts in the AP_F,[a] AP_P, and AP_E 9-mer Duplexes at 5 °C

	chemical shifts (ppm) P	H3′[b]	H4′[b]	H2′,2″[b]	H4′[c]	H5′,5″[c]
AP_F 9-mer						
A5-G6[d]	−3.70	4.87				4.37
C13-F14[d]	−3.28	4.80	4.18	2.17, 2.29	4.18	3.91, 4.01
F14-C15[d]	−3.77	4.61	4.16	1.95	4.25	4.34
AP_P 9-mer						
A5-G6[d]	−3.57	4.84				4.33
C13-P14	−3.01	4.81			1.88	3.93
P14-C15	−2.78	3.91	1.88			4.24
AP_E 9-mer						
A5-G6[d]	−3.47	4.85				
C13-E14	−3.05	4.84				3.98
E14-C15	−2.80	3.98				

[a] Data not shown. [b] O3′-Linked ^{31}P–^1H correlations. [c] O5′-Linked ^{31}P–^1H correlations. [d] These phosphodiester resonances have also been assigned by specific ^{17}O labeling.

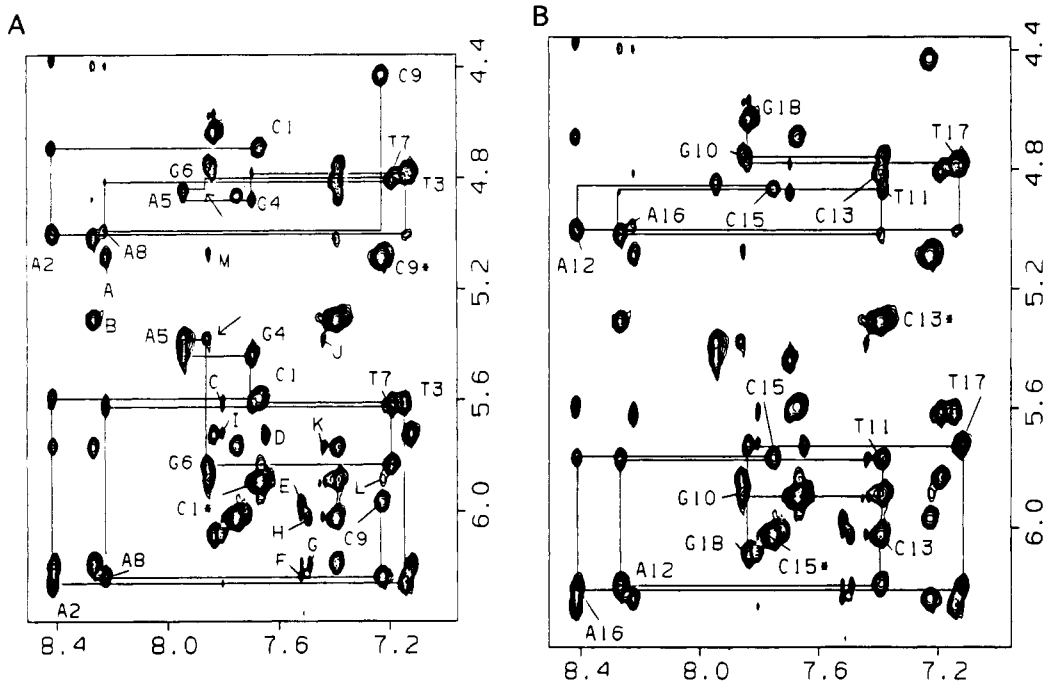

FIGURE 2: Expanded contour plots of the phase-sensitive NOESY spectrum (mixing time 250 ms) of the AP_P 9-mer duplex in 0.1 M NaCl, 10 mM phosphate, and D_2O, pH 6.7, at 5 °C. Distance connectivities between the base protons (7.0–8.5 ppm) and the sugar H1′ and H3′ protons (4.4–6.4 ppm) for the unmodified d(C1-A2-T3-G4-A5-G6-T7-A8-C9) strand are plotted in (A) and for the modified d(G10-T11-A12-C13-P14-C15-A16-T17-G18) strand are plotted in (B). The cytidine H6–H5 crosspeaks are designated by asterisks. The crosspeaks A–M are discussed in the text. The lines follow connectivities between adjacent base protons and their intervening sugar H1′ and H3′ protons in each strand of the AP_P 9-mer duplex.

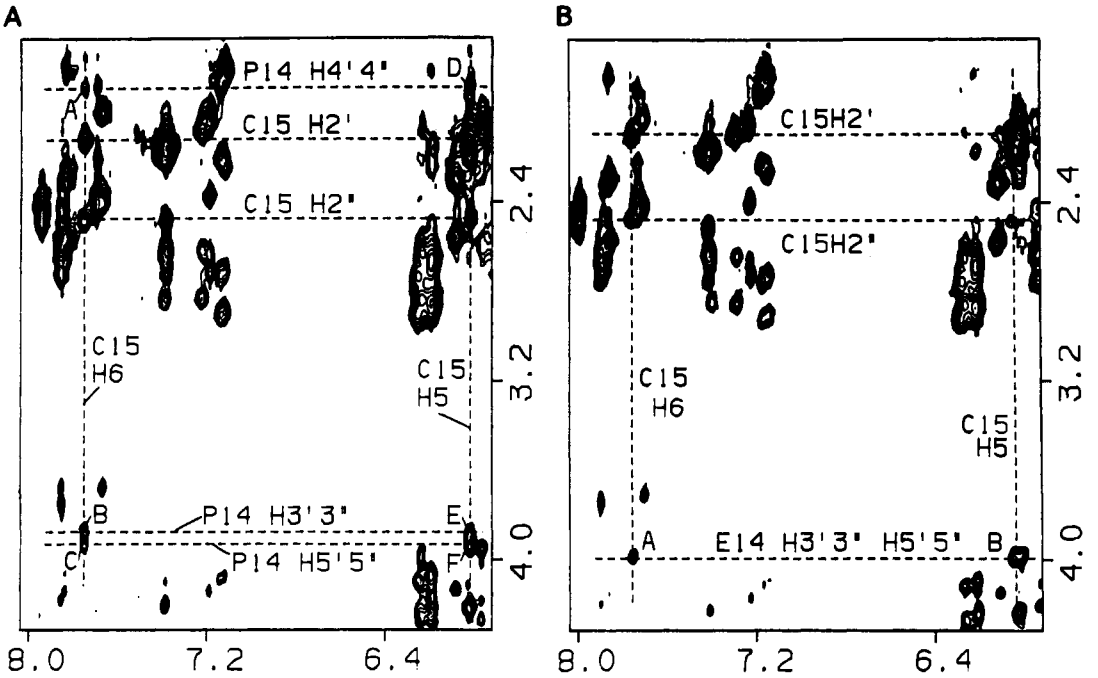

FIGURE 3: An expanded NOESY contour plot of (A) the AP_P 9-mer duplex in 0.1 M NaCl, 10 mM phosphate, and D_2O at 5 °C and (B) the AP_E 9-mer duplex in 0.1 M NaCl, 10 mM phosphate, and D_2O at 5 °C establishing distance connectivities between the 6.0–8.0-ppm and the 1.8–4.2-ppm spectral regions. The crosspeaks A–F in (A) and the crosspeaks A and B in (B) are discussed in the text.

Coupling and distance connectivities between the H3′,3″ and the H4′,4″ protons, between the H5′,5″ and the H4′,4″ protons, and between the H3′,3″ and the H5′,5″ protons are observed in the magnitude COSY and NOESY spectra. Several NOEs are observed involving propanyl protons of residue P14 and the adjacent C15 base protons in the AP_P 9-mer duplex. An expanded region of the NOESY spectrum between the H6 and H5 protons of residue C15 (5.9–8.0 ppm) and the abasic-site protons (1.8–4.4 ppm) is plotted in Figure 3A. In right-handed DNA, pyrimidine H5 and H6 protons display directional NOEs to their own and 5′-linked sugar protons. These directional NOEs are observed as weak crosspeaks between P14 protons and the H6 protons of C15 (crosspeaks A–C, Figure 3A) and the H5 protons of C15 (crosspeaks D–F, Figure 3A).

Phosphorus Spectra. The 121.5-MHz proton Waltz-decoupled phosphorus spectrum of the AP_P 9-mer duplex in H_2O solution at 5 °C is shown at the top of Figure 4. The majority of the 16 backbone phosphates resonate between −4.0 and −4.5 ppm within the characteristic range of unperturbed phos-

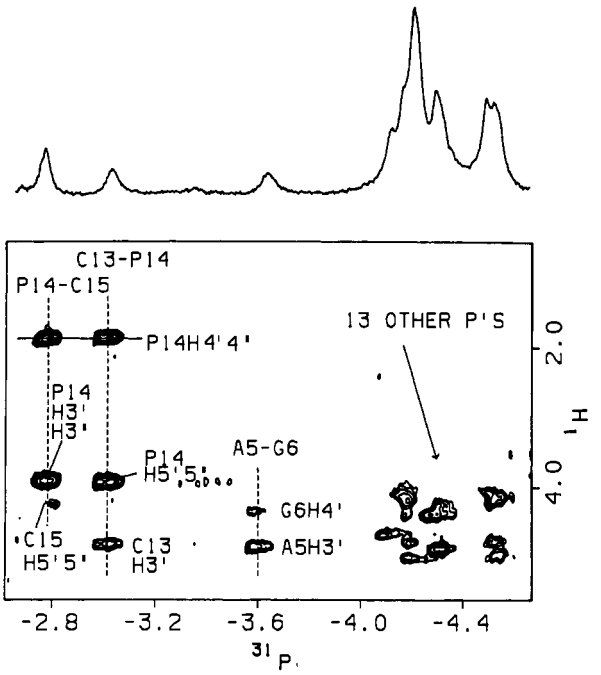

FIGURE 4: Two-dimensional heteronuclear phosphorus (observe)–proton COSY contour plot of the AP_P 9-mer duplex, D_2O solution at 5 °C. Note that only the positive contour levels are plotted for clarity, and the reference is also to the positive contours.

phodiester backbone resonances. Three resonances are observed at −2.78, −3.01, and −3.59 ppm and have been assigned to the P14-C15, C13-P14, and A5-G6 backbone phosphates in AP_P 9-mer, respectively, by analyzing the phosphorus–proton heteronuclear COSY experiment (Figure 4).

AP_E 9-mer Duplex

The proton spectra of the AP_E 9-mer duplex are very similar to those of the AP_P 9-mer duplex. Assignments were made with the experimental protocol outlined above.

Exchangeable Protons. The expanded regions of the NOESY spectrum (mixing time 120 ms) recorded at 0 °C in H_2O of the AP_E 9-mer are given in Figure 5, and the assignments of the exchangeable protons are explained in the figure caption. The chemical shift values are tabulated in Table II. Each of the four thymidine imino protons resonating between 13.5 and 13.7 ppm develops a strong NOE to the adenosine H2 proton within the base pair (peaks E–H, Figure 5B), establishing Watson–Crick base pairing of the four A·T base pairs. Each of the four guanosine imino protons resonating between 12.3 and 12.8 ppm develops a strong NOE to the hydrogen-bonded and exposed cytidine amino protons within the base pair (peaks J–M, I, P, and V, Figure 5B), establishing Watson–Crick base pairing of the G·C base pairs. NOEs are also detected between the imino protons of adjacent base pairs (crosspeaks A–D, Figure 5A). These eight imino protons broaden as the temperature is raised above 15 °C, reflecting the onset of the melting transition.

Focusing on the d(G4-A5-G6)·d(C13-E14-C15) segment, two NOE crosspeaks are detected which involve unresolved imino protons and adenosine H2 protons. Both the G4 and G5 imino protons develop NOEs to the H2 proton on A5 (crosspeaks Q and O, respectively, Figure 5B). However, ambiguities arise since an NOE between the imino proton of G10 and the H2 proton of A8 resonates coincident with crosspeak Q and an NOE between the imino proton of G5 and the H2 proton of A12 resonates coincident with crosspeak O in Figure 5B. One-dimensional NOE difference spectra were

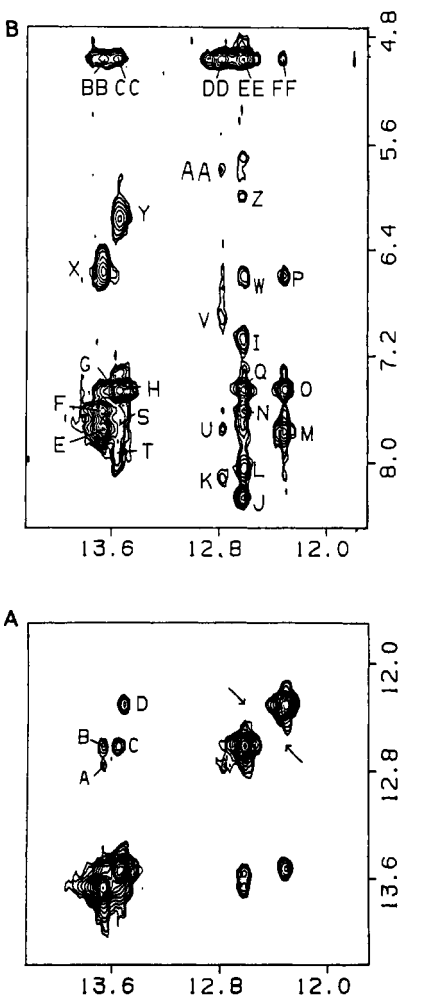

FIGURE 5: Expanded phase-sensitive NOESY (120-ms mixing time) contour plots of the AP_E 9-mer duplex in 0.2 M NaCl, 20 mM phosphate, and H_2O, pH 6.15, at 0 °C. (A) Crosspeaks establishing connectivities between imino protons in the symmetrical 12.0–14.0-ppm spectral range. (B) Crosspeaks establishing connectivities between imino protons (12.0–14.0 ppm) and the base and amino protons (4.8–8.5 ppm). The crosspeaks A–FF are assigned as follows: The 13.67-ppm imino proton of T17 exhibits NOE crosspeaks to the imino proton of G18 (peak A) and to the H2 proton (peak E) and exposed amino proton of A2 (peak X). The 13.66-ppm imino proton of T3 exhibits NOE crosspeaks to the imino proton of G4 (peak B) and to the H2 proton (peak F) and exposed amino proton of A16 (peak X). The NOE crosspeaks involving the thymidine imino proton and the adenosine hydrogen-bonded amino proton within the A2·T17 and T3·A16 base pairs resonate at the same positions as the NOE crosspeaks between the thymidine imino protons and the adenosine H2 protons within the same two base pairs (peaks E and F, respectively). The 13.55-ppm imino proton of T11 exhibits NOE crosspeaks to the amino proton of G10 (peak C) and to the hydrogen-bonded (peak T) and exposed (peak Y) amino protons and H2 proton of A8 (peak G). The 13.51-ppm imino proton of T7 exhibits NOE crosspeaks to the imino proton of G6 (peak D) and to the hydrogen-bonded (peak S) and exposed (peak Y) amino protons and H2 proton (peak H) of A12. The 12.75-ppm imino proton of G18 exhibits NOE crosspeaks to the hydrogen-bonded (peak K) and exposed (peak V) amino protons and H5 proton (peak AA) of C1 and to the H2 proton of A2 (peak U). The 12.61-ppm imino proton of G10 exhibits NOE crosspeaks to the hydrogen-bonded (peak L) and exposed (peak W) amino protons of C9 and to the H2 proton of A8 (peak Q). The 12.62-ppm imino proton of G4 exhibits NOE crosspeaks to the hydrogen-bonded (peak J) and exposed (peak I) amino protons and H5 proton (peak Z) of C15 and to the H2 protons of A16 (peak N) and A5 (peak Q). The 12.30-ppm imino proton of G6 exhibits NOE crosspeaks to the hydrogen-bonded (peak M) and exposed (peak P) amino protons of C13 and to the H2 protons of A5 (peak O) and A12 (peak O). Crosspeaks BB–FF arise due to chemical exchange of each of the imino protons with the H_2O solvent during the mixing time.

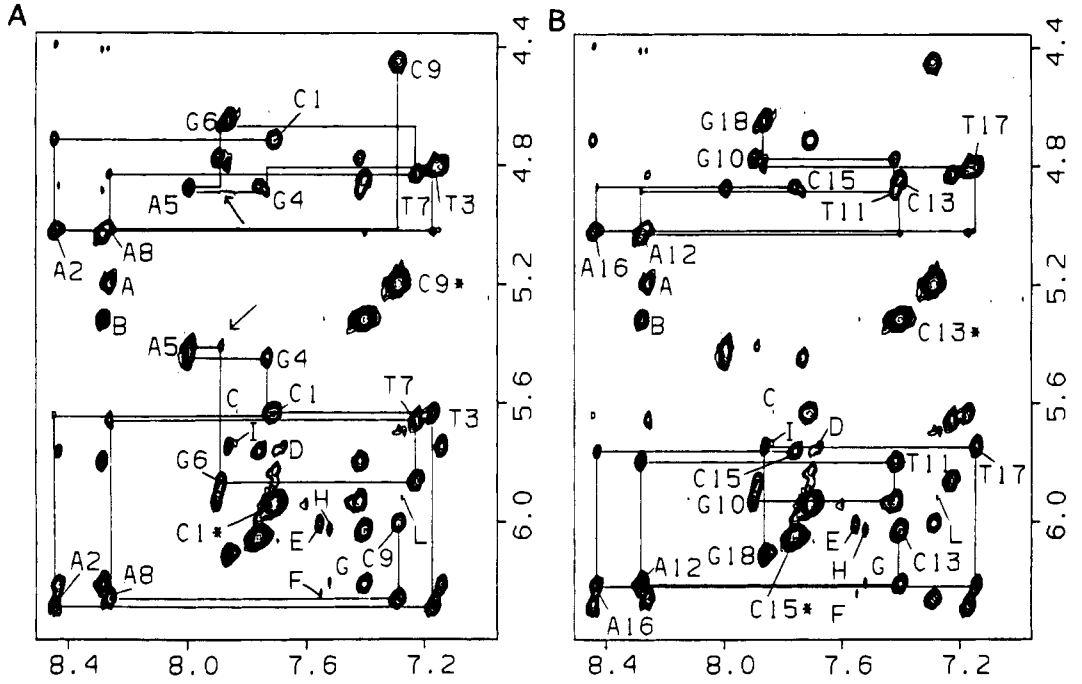

FIGURE 6: Expanded contour plots of the phase-sensitive NOESY spectrum (mixing time 250 ms) of the AP_E 9-mer duplex in 0.1 M NaCl, 10 mM phosphate, and D_2O, pH 6.3, at 5 °C. Distance connectivities between the base protons (7.0–8.5 ppm) and the sugar H1′ and H3′ protons (4.4–6.4 ppm) for the unmodified d(C1-A2-T3-G4-A5-G6-T7-A8-C9) strand are plotted in (A) and for the modified d(G10-T11-A12-C13-E14-C15-A16-T17-G18) strand are plotted in (B). The cytidine H6–H5 crosspeaks are designated by asterisks. The crosspeaks A–G are discussed in the text. The lines follow connectivities between adjacent base protons and their intervening sugar H1′ and H3′ protons in each strand of the AP_P 9-mer duplex.

recorded at −5 and 5 °C but were unsuccessful in resolving these ambiguities.

Nonexchangeable Protons. The expanded regions of the NOESY spectrum (250-ms mixing time) at 5 °C in D_2O of the AP_E 9-mer duplex involving the base and sugar H1′ and H3′ protons are given in Figure 6. The assignments are nearly identical with those of the AP_P 9-mer duplex. The unmodified strand can be traced without interruption from the 5′-end to the 3′-end (Figure 6A). The modified strand can be traced except at the modification site, since none of the protons of the ethanyl moiety resonate between 4.4 and 8.6 ppm (Figure 6B). The tracing is perturbed at the A5-G6 step (see arrows, Figure 6A). NOE crosspeaks are observed at the purine H8/pyrimidine H5/CH_3 steps for the A2-T3, G6-T7, A8-C9 (crosspeak A, Figure 6A), G10-T11, A12-C13 (crosspeak B, Figure 6B), and A16-T17 steps in the AP_E 9-mer duplex. Adenosine H2 protons display NOEs to their own, 3′-adjacent, and cross-strand sugar H1′ protons (crosspeaks C–I, Figure 6). The majority of the remaining NOE crosspeaks have been assigned in the AP_E 9-mer and confirmed by analyzing the coupling connectivities linking the sugar protons in the COSY spectrum. The chemical shift values of the base and sugar H1′, H2′,2″, H3′, and most of the H4′ protons for the AP_E 9-mer at 5 °C are given in Table II.

The proton resonances of the abasic site ethanyl moiety have been identified via the strong heteronuclear correlations to the ^{31}P atoms in the phosphodiester backbone (see next section). The H3′,3″ and H5′,5″ protons of E14 resonate at the same chemical shift of 3.99 ppm. The H6 and H5 protons of C15 develop NOEs to their own and 5′-linked H3′,3″ and H5′,5″ protons of E14 (crosspeaks A and B, Figure 3B).

Phosphorus Spectra. The 121.5-MHz proton Waltz-decoupled phosphorus spectrum of the AP_E 9-mer duplex in D_2O solution at 5 °C is shown at the top of Figure 7. The majority of the 16 backbone phosphates fall within the characteristic range of unperturbed phosphodiester backbone resonances (−4.0 and −4.5 ppm). Three resonances are observed at −2.80, −3.05, and −3.47 ppm which have been assigned to the E14-C15, C13-E14, and A5-G6 backbone phosphates, respectively, in the AP_E 9-mer, by analyzing the phosphorus–proton heteronuclear COSY experiment (Figure 7).

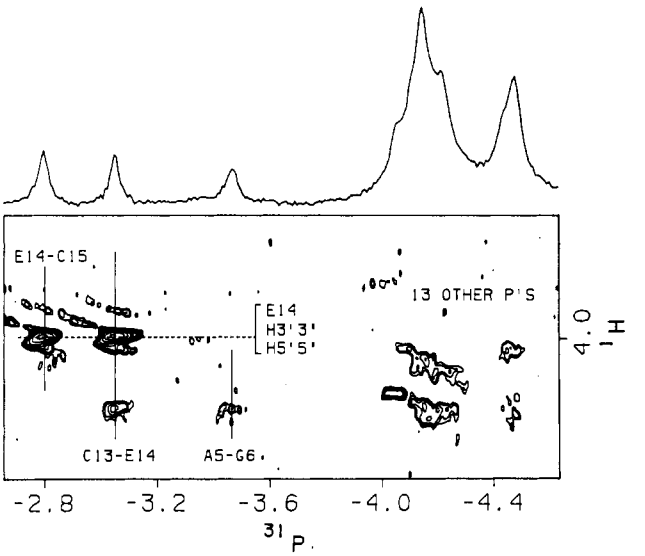

FIGURE 7: Two-dimensional heteronuclear phosphorus (observe)–proton COSY contour plot of the AP_E 9-mer duplex, D_2O solution at 5 °C. Note that only the positive contour levels are plotted for clarity, and the reference is also to the positive contours.

DISCUSSION

Abasic sites in DNA may play an important role in events leading to spontaneous and chemically induced mutagenesis and carcinogenesis. Additional insights into the recognition, interaction, and repair of the abasic site by DNA polymerases and AP endonucleases may be revealed by a more complete understanding of the structural features of the abasic site, including contributions from the base opposite the lesion and

the sequence of the flanking base pairs. The current NMR study uses propanyl (structure 4) and ethanyl (structure 5) analogues of the open aldehyde form of the naturally occurring abasic site (structure 2) embedded in the center of a nonanucleotide duplex with deoxyadenosine located opposite the abasic site (AP_P 9-mer and AP_E 9-mer duplexes, structure 6 and 7). The only structural difference between the AP_P 9-mer and AP_E 9-mer duplexes is that the acyclic analogue is shortened by one carbon atom in the latter. The solution NMR results indicate that both the AP_P 9-mer and AP_E 9-mer duplexes form stable right-handed helices at low temperatures (0 °C). The majority of the base and sugar protons were assigned by analyzing through-space connectivities observed in the two-dimensional NOESY experiments and through-bond connectivities observed in two-dimensional COSY experiments. The base and sugar proton chemical shifts for both duplexes are given in Tables I and II. Results of our studies permit differentiation of Watson–Crick and Hoogsteen base pairing, right- and left-handed DNA, syn- and anti-glycosidic torsion angles, stacking and looping out of bases, and normal and perturbed phosphate backbones. Interpretations of NMR experiments on complex macromolecules are strengthened when comparative studies are conducted on several molecules differing in a single important aspect. Hence, parallel studies have been conducted on the parent A·T 9-mer duplex (structure 8, unpublished results) and on the AP_F 9-mer duplex (structure 9), which corresponds to a cyclic analogue (structure 3) of the abasic site (structure 1) located at the center of an otherwise identical nonamer duplex (Kalnik et al., 1988).

Base Pairing. The observed NOEs between each thymidine imino proton and the adenosine H2 proton within the base pair establishes Watson–Crick pairing for the A·T base pairs, and the observed NOEs between each guanosine imino proton and the hydrogen-bonded cytidine amino proton within the base pair establish Watson–Crick hydrogen bonding for the G·C base pairs for th AP_P 9-mer and AP_E 9-mer duplexes at low temperature (Figures 1 and 5). These data clearly demonstrate that the two G·C base pairs flanking the abasic site in the AP_P and AP_E 9-mer duplexes are intact at low temperatures. The imino proton spectra and NOE connectivities observed for the AP_F 9-mer are very similar to those observed for the AP_P 9-mer and AP_E 9-mer duplexes, demonstrating that neither the absence of an intact deoxyribose ring nor a shortened backbone at the abasic site has any significant effect on hydrogen bonding of the two flanking base pairs.

Base Stacking and Helix Handedness. The directional NOEs observed between the purine H8 and pyrimidine H6 protons and their own and 5′-linked sugar H1′, H2′, H2″, and H3′ protons in the AP_P 9-mer and AP_E 9-mer duplexes demonstrate that the helices are right-handed and the base pairs are stacked in aqueous buffer solution at 5 °C. The observation of directional NOEs between the H2 protons of adenosine and nearby sugar protons and between base protons in purine (3′–5′)pyrimidine steps (Figures 2 and 6) substantiates the conclusion that all of the residues are stacked and in a right-handed conformation in both duplexes.

Glycosidic Torsion Angles. The conformation of the glycosidic bond can be determined by monitoring the NOE between the base proton and its own sugar H1′ proton. If the glycosidic torsion angle is syn, the sugar H1′ proton is within 2.5 Å of the base proton (purine H8 or pyrimidine H6) and develops a strong NOE comparable in intensity to that of the NOE observed between the fixed-distance (2.45 Å) cytidine H5 and H6 protons. When the glycosidic torsion angle is anti, the sugar H1′ proton is ~3.7 Å from its own base proton, and the NOE predicted would be much weaker than the NOE detected between the cytidine H5 and H6 protons (Patel et al., 1983). All 17 intranucleotide base to H1′ NOEs have much weaker intensities in NOESY spectra recorded with a 250-ms mixing time (Figures 2 and 6) and recorded with a 50-ms mixing time (data not shown) relative to any of the NOEs between cytidine H5 and H6 protons, establishing an anti conformation of all 17 glycosidic torsion angles in both the AP_P 9-mer and AP_E 9-mer duplexes.

Stacking of Residue A5 opposite the Abasic Site. The orientation of the A5 residue opposite the abasic site was determined by monitoring NOEs involving the H2 proton of residue A5 and protons of flanking base pairs. In both one- and two-dimensional NOE experiments conducted on the AP_P 9-mer duplex, the G4 imino proton of the G4·C15 base pair displays NOEs of similar magnitude to those of the H2 protons of the flanking A5 and A16 residues (Figure 1). Similarly, the G6 imino proton of the G6·C13 base pair also displays NOEs of similar magnitude to those of the partially resolved H2 protons of the adjacent A5 and A12 residues (Figure 1). These NOEs establish that the A5 residue inserts into the helix and stacks with the adjacent G4·C15 and G6·C13 base pairs in the AP_P 9-mer duplex. In the AP_E 9-mer duplex spectral overlap of three adenosine H2 protons and two of the guanosine imino protons prevents unambiguous demonstration of the stacking of the A5 residue into the helix, although the observed pattern of NOEs is consistent with A5 stacking into the helix. The stacking of the A5 residue into the helix causes the G4·C15 and G6·C13 base pairs to be separated, which is consistent with the absence of an NOE between the G4 and G6 imino protons in the AP_P 9-mer duplex (Figure 1A, see arrows) and the AP_E 9-mer duplex (Figure 5A, see arrows).

In both the AP_P 9-mer and AP_E 9-mer duplexes the distance connectivities between purine H8 protons and their own and 5′-flanking sugar protons can be traced in the G4-*A5*-G6 segment. However, the NOEs between the H8 proton of residue G6 and the sugar protons of residue A5 are weak (see arrows in Figures 2A and 6A), suggesting a conformational perturbation at the A5-G6 step in both duplexes. The relative weakness of the NOE signal between the H8 proton of G6 and the H1′ proton of A5 may reflect a somewhat extended structure at the A5-G6 step, a perturbation in the A5 glycosidic bond in the anti range, or an abnormal conformation of the A5 sugar moiety.

Base protons experience large upfield shifts due to ring current effects upon base stacking in the duplex. The H2 and H8 protons of residue A5 (7.44 and 7.94 ppm in the AP_P 9-mer duplex, respectively, and 7.46 and 7.99 ppm in the AP_E 9-mer duplex, respectively) exhibit the most upfield chemical shifts relative to all the other adenosine base protons. These upfield shifts of the A5 base protons also demonstrate that the A5 residue is stacked into the helix for both the AP_P 9-mer and AP_E 9-mer duplexes.

Comparison of the Cyclic and Acyclic Abasic Site Analogues. Exchangeable and nonexchangeable proton spectra are nearly identical for the cyclic AP_F 9-mer and acyclic AP_P 9-mer duplexes. The only chemical shift differences greater than 0.05 ppm for the (G4-A5-G6)·(C13-F/P14-C15) trinucleotide segment between the two duplexes occur at the H5 (−0.06 ppm), sugar H2′ (−0.10 ppm), hydrogen-bonded amino (−0.07), and exposed amino (−0.11 ppm) protons of residues C15 and the sugar H2″ (0.11 ppm) proton of residue C13 when proceeding from the AP_F 9-mer duplex to the AP_P 9-mer duplex. These chemical shift differences are relatively small and indicate that the base pairs flanking the abasic site are

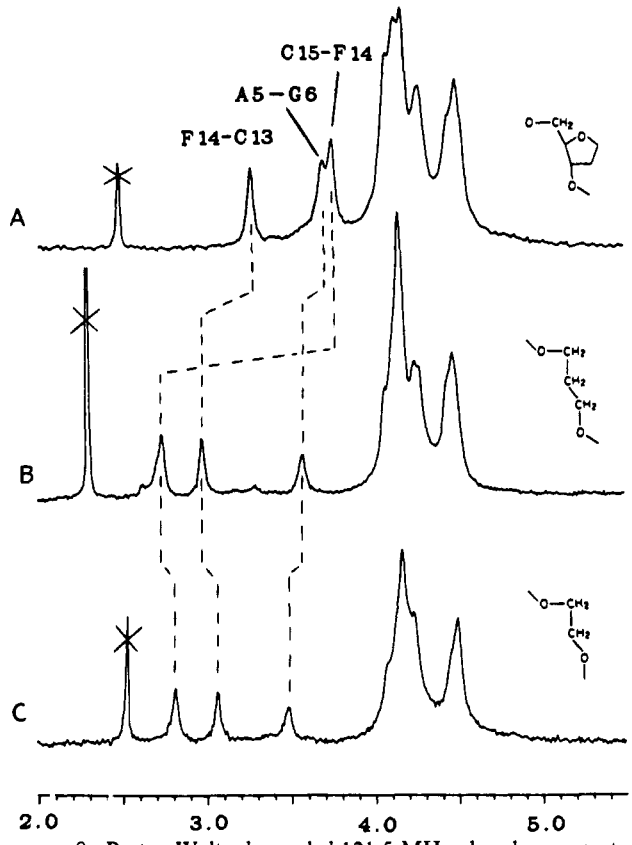

FIGURE 8: Proton Waltz-decoupled 121.5-MHz phosphorus spectra (−2.0 to −5.5 ppm) of (A) the AP_F 9-mer duplex in 0.1 M NaCl, 10 mM phosphate, and D_2O, pH 6.6, at 5 °C; (B) the AP_P 9-mer duplex in 0.1 M NaCl, 10 mM phosphate, and D_2O, pH 6.6 at 5 °C; and (C) the AP_E 9-mer duplex in 0.2 M NaCl, 20 mM phosphate, and D_2O, pH 6.6, at 5 °C. The resonances designated by an X arise from the phosphate buffer.

intact and assume similar conformations in both the AP_F 9-mer and AP_P 9-mer duplexes. Both duplexes show a disruption in the proton NOE connectivities between the G6 base protons and the A5 sugar protons. These through-space connectivities are much weaker than those observed throughout the rest of the helix.

The ^{31}P spectra of the AP_F 9-mer and AP_P 9-mer duplexes differ in the pattern of their downfield-shifted resonances. Both the AP_F 9-mer and AP_P 9-mer duplexes have three resonances shifted downfield of the chemical shift range of unperturbed phosphodiester backbone resonances (panels A and B of Figure 8, respectively). The C15-F/P14 resonance shifts 0.99 ppm downfield when proceeding from the AP_F 9-mer to the AP_P 9-mer duplex, while the F/P14-C13 resonance shifts 0.27 ppm downfield and the A5-G6 resonance shifts 0.13 ppm downfield, indicating that the backbone may assume a different conformation in the two duplexes.

Comparison of the Ethane and Propane Acyclic Abasic Site Analogues. Focusing on the central d(G4-A5-G6)·d(C13-P/E14-C15) region, all of the chemical shift differences between the AP_P 9-mer and AP_E 9-mer duplexes are less than 0.10 ppm. The amino protons of both C13 and C15 are shifted slightly upfield as one proceeds from the AP_P duplex to the AP_E duplex. The exchangeable protons of the terminal base pairs also shift slightly upfield which is likely due to the difference in the NaCl concentration of the H_2O sample buffers for the AP_P 9-mer (0.1 M) and AP_E 9-mer (0.2 M) duplexes. The imino proton resonances of the AP_E 9-mer duplex exhibit line broadening at 15 °C, at a slightly lower temperature than in the AP_P 9-mer duplex. The distortions of the through-space proton connectivities at the A5-G6 step are the most pronounced for the AP_E 9-mer duplex. The absence of these NOEs reflects the changes in the opposite strand due to the shortening of the backbone at residue E14. A similar disruption of the NOE connectivities was observed in an adenosine bulge containing duplex with the following sequence at the bulge site: d(G3-AX-G4)·d(C9-C10) (Kalnik et al., 1989). The NOE connectivities observed between the base protons of residue G4 and the sugar protons of AX were weak. The bulge adenosine also stacks within the duplex even after the removal of the entire nucleotide unit.

The ^{31}P spectrum of the AP_E 9-mer is very similar to that of the AP_P 9-mer with the exception that the A5-G6 phosphodiester resonance shifts 0.10 ppm downfield. These results indicate that the conformation of the phosphodiester backbone at the lesion site is very similar for the AP_P 9-mer and AP_E 9-mer duplexes. These results are somewhat surprising since in vitro studies demonstrate that the propanyl and ethanyl moieties behave quite differently with respect to AP endonuclease action (Takeshita et al., 1988).

Biological Implications. Abasic sites have been implicated as intermediates in spontaneous and chemically induced mutagenesis (Loeb & Preston, 1987). The present NMR studies indicate that the deoxyadenosine residue opposite the abasic site is stacked into the helix while the flanking base pairs remain intact. These observations are consistent with the in vivo and in vitro studies in which dAMP is shown to be preferentially incorporated opposite the abasic site, leading to base-substitution mutations in the daughter strands (Sagher & Strauss, 1983). If the deoxyadenosine opposite the abasic site were looped out of the helix, allowing flanking base pairs to stack with each other, a frameshift mutation would be expected to occur (Fresco & Alberts, 1960).

The most significant structural implications of this study are that the propanyl and ethanyl moieties adopt very similar conformations within duplex DNA in solution and that the helical structure of duplex DNA is maintained after removal of the base, the 2-deoxyribose moiety, and even one of the backbone carbon atoms. Base pairing and stacking are similar in the cyclic and the acyclic abasic site analogue duplexes, suggesting that stacking interactions adjacent to the lesion and further along the helix play an important role in preserving the conformation of the DNA in solution.

ACKNOWLEDGMENTS

We gratefully acknowledge the assistance of Robert Rieger in the large-scale preparation of modified oligodeoxynucleotides.

Registry No. AP_P 9-mer duplex, 119147-15-8; AP_E 9-mer duplex, 119147-17-0; deoxyadenosine, 958-09-8.

REFERENCES

Bax, A., & Davis, D. (1985) *J. Magn. Reson. 65*, 355–360.
Fresco, J. R., & Alberts, B. M. (1960) *Proc. Natl. Acad. Sci. U.S.A. 46*, 311–321.
Hare, D. R., Wemmer, D. E., Chou, S. H., Drobny, G., & Reid, B. R. (1983) *J. Mol. Biol. 171*, 319–336.
Hore, P. J. (1983) *J. Magn. Reson. 55*, 283–300.
Kalnik, M. W., Chang, C. N., Grollman, A. P., & Patel, D. J. (1988) *Biochemistry 27*, 924–931.
Kalnik, M. W., Norman, D. G., Swann, P. F., & Patel, D. J. (1989) *J. Biol. Chem.* (in press).
Klevitt, R. E. (1985) *J. Magn. Reson. 62*, 551–555.
Lindahl, T. (1982) *Annu. Rev. Biochem. 51*, 61–87.
Loeb, L. A. (1985) *Cell 40*, 483–484.
Loeb, L. A., & Kunkel, T. A. (1982) *Annu. Rev. Biochem. 52*, 429–547.

Loeb, L. A., & Preston, B. D. (1987) *Annu. Rev. Genet. 20*, 201–230.
Otting, G., Widmer, H., Wagner, G., & Wuthrich, K. (1986) *J. Magn. Reson. 66*, 187–193.
Patel, D. J., Kozlowski, S. A., Nordheim, A., & Rich, A. (1983) *Proc. Natl. Acad. Sci. U.S.A. 79*, 1413–1417.
Plateau, P., & Gueron, M. (1982) *J. Am. Chem. Soc. 104*, 7310–7311.
Sagher, D., & Strauss, B. (1983) *Biochemistry 22*, 4518–4526.
Scheek, R. M., Boelens, R., Russo, N., van Boom, J. H., & Kaptein, R. (1984) *Biochemistry 23*, 1371–1376.
Shaka, A. J., Keeler, J., Frenkiel, T., & Freeman, R. (1983) *J. Magn. Reson. 52*, 335–338.
States, D. J., Haberkorn, R. A., & Ruben, D. J. (1982) *J. Magn. Reson. 48*, 286–292.
Takeshita, M., Chang, C. N., Johnson, F., Will, S., & Grollman, A. P. (1987) *J. Biol. Chem. 262*, 10171–10179.
Weiss, B., & Grossman, L. (1987) *Adv. Enzymol. 60*, 1–34.
Weiss, M. A., Patel, D. J., Sauer, R. T., & Karplus, M. (1984) *Proc. Natl. Acad. Sci. U.S.A. 81*, 130–134.
Zagorski, M. G., & Norman, D. G. (1989) *J. Magn. Reson.* (in press).

Picosecond Tryptophan Fluorescence of Thioredoxin: Evidence for Discrete Species in Slow Exchange†

Fabienne Mérola,‡,§ Rudolf Rigler,‡ Arne Holmgren,*,‖ and Jean-Claude Brochon§

Departments of Medical Biophysics and Physiological Chemistry, Karolinska Institutet, Box 60400, S-10401 Stockholm, Sweden, and Laboratoire pour l'Utilisation du Rayonnement Electromagnétique, CNRS-MEN-CEA, Bat. 209D, Université Paris Sud, F-91405 Orsay, France

Received August 11, 1988; Revised Manuscript Received December 20, 1988

ABSTRACT: The steady-state tryptophan fluorescence and time-resolved tryptophan fluorescence of *Escherichia coli* thioredoxin, calf thymus thioredoxin, and yeast thioredoxin have been studied. In all proteins, the tryptophan residues undergo strong static and dynamic quenching, probably due to charge-transfer interactions with the nearby sulfur atoms of the active cysteines. The use of a high-resolution photon counting instrument, with a time response of 60 ps full width at half-maximum, allowed the detection of fluorescence lifetimes ranging from a few tens of picoseconds to 10 ns. The data were analyzed both by classical nonlinear least squares and by a new method of entropy maximization (MEM) for the recovery of lifetime distributions. Simulations representative of the experimental data were used to test the MEM analysis. Strong support was obtained in this way for a small number of averaged discrete species in the fluorescence decays. Wavelength studies show that each of these components spreads over closely spaced excited states, while the temperature studies indicate that they do not exchange significantly on the nanosecond time scale. The oxidized form of thioredoxin is characterized by a high content of a very short lifetime below 70 ps, the amplitude of which is sharply decreased upon reduction. On the other hand, the fluorescence anisotropy decays indicate that reduction causes an increase of the very fast tryptophan rotations in an otherwise relatively rigid structure. While the calf thymus and *E. coli* proteins have mostly similar dynamical fluorescence properties, the yeast thioredoxin differs in many respects.

Thioredoxin is a small (M_r 11 700), ubiquitous protein with a redox-active cystine in its oxidized form, Trx-S_2.[1] Reduction of Trx-S_2 by NADPH and thioredoxin reductase gives the reduced form Trx-$(SH)_2$ with a dithiol. Thioredoxin functions in many important biological processes as an enzyme catalyzing dithiol–disulfide exchange with proteins (Gadal et al., 1983; Holmgren, 1985; Holmgren et al., 1986). Thioredoxin from *Escherichia coli* is the best characterized molecule, with its amino acid sequence of 108 residues known (Holmgren, 1968) and the three-dimensional structure of Trx-S_2 solved by X-ray crystallography to 2.8-Å resolution (Holmgren et al., 1975). The molecule has a high content of secondary structure, with five strands of β-pleated sheet and four α-helices, and the active site located in a protruding part of the structure. From the homology of primary structures, all cellular thioredoxins probably share this common fold as well as the conserved sequence of its 14-membered active disulfide ring: Trp31-Cys-Gly-Pro-Cys-Lys36 (Holmgren, 1985; Gleason & Holmgren, 1988).

The structure of Trx-$(SH)_2$ is less well-known since it has not been crystallized. Reduction does not bring significant changes in the UV absorption spectra, the ORD, and the CD spectra in the far UV (Stryer et al., 1967; Reutimann et al., 1981), while it gives a 3-fold increase in the tryptophan fluorescence emission (Stryer et al., 1967; Holmgren, 1972;

† Work supported by grants from the Swedish National Science Research Council (K-KU 3167-303) and the Swedish Medical Research Council (13X-3529). F.M. was the recipient of a postdoctoral grant from the Wenner-Gren Foundation (Sweden) during her stay at the Karolinska Institute.

* To whom correspondence should be addressed.
‡ Department of Medical Biophysics, Karolinska Institutet.
§ CNRS-MEN-CEA.
‖ Department of Physiological Chemistry, Karolinska Institutet.

[1] Abbreviations: FWHM, full width at half-maximum; MEM maximum entropy method; Trx-S_2, Trx-$(SH)_2$, the oxidized and the reduced forms, respectively, of thioredoxin; NADPH, nicotinamide adenine dinucleotide phosphate (reduced); DTT, dithiothreitol; ORD optical rotatory dispersion; CD circular dichroism; UV ultraviolet; NMR, nuclear magnetic resonance; DTNB, 5,5′-dithiobis(2-nitrobenzoic acid); NATA, *N*-acetyltryptophanamide; Boc, *tert*-butyloxycarbonyl; NHMe, methylamide.

0006-2960/89/0428-3383$01.50/0